# Supplemental material

Ma et al., https://doi.org/10.1085/jgp.201912460

## Supplemental results and discussion

### *Mouse SOL and EDL*

We wanted to test the generality of our conclusions concerning lattice/fiber type correlation, based on our rat observations, by studying the same question in mice using x-ray diffraction and EM. The mouse is more difficult because its EDL and SOL have a greater mix of fiber types. While the EDL is ∼100% fast (66% IIB, 21% IIDB, 8% IIAD [Augusto et al., 2004]), the SOL is not a "pure" muscle, but a mixture of 60–70% fast and 30–40% slow (Wigston and English, 1992). Various studies have estimated fiber type amounts as: 37% type I, 39% IIA, 19% IIAD (Augusto et al., 2004); 40% I, 50% IIA, 5% IIB/X (Luedeke et al., 2004); and 34% I, 59% IIA, 6% IIB, 1% IIC (Totsuka et al., 2003).

If slow (type I) fibers have a simple lattice, and fast (type IIB/X/D) have a superlattice, as suggested by the rat results, this would predict a superlattice pattern for mouse EDL. However, the prediction for mouse SOL will depend on the lattice arrangement in type IIA fibers, as this is the predominant fiber type in mouse SOL. As discussed in the text, results from mouse diaphragm suggest that type IIA fibers have a simple lattice (Iwamoto et al., 2003).

The x-ray results were suggestive, but not definitive. Mouse EDL showed little or no sampling on ML1, consistent with a superlattice that is very limited in extent and/or poorly ordered (Fig. S6, B and E). Mouse SOL showed diffuse sampling on ML1 aligned with the 1,1 equatorial reflection (the strongest sampled reflection in rat SOL), while the rest of the layer line was unsampled. This is consistent with the presence of a simple lattice in a substantial fraction of fibers in mouse SOL. However, the diffuseness of the 1,1 sampling, and the absence of sampling along the rest of the layer line, suggest that the simple lattice is not extensive/highly ordered and/or that some fibers in mouse SOL do not have a simple lattice. Lack of ordering seems more likely if we assume that type IIA fibers have a simple lattice. This possibility is supported by our observation that when mouse SOL was treated with blebbistatin, known to improve the ordering of myosin heads on the thick filaments, the sampling on the 1,1 row line became sharper, and a second spot appeared on the 1,0 row line (the second strongest sampled reflection in rat; Fig. S7, B and D). This suggests the presence of an (imperfectly ordered) simple lattice in most of the fibers in mouse SOL, supporting the view that both type I and IIA fibers have a simple lattice. This conclusion is also suggested by rat SOL, which, while containing up to 15% type IIA fibers (Wigston and English, 1992; Li et al., 2019), shows a clear simple lattice, with no obvious sign of a superlattice. In contrast with the SOL, mouse EDL showed no change in sampling with blebbistatin. Further support for the presence of a simple lattice in type I and IIA fibers in mouse comes from examination of diffraction patterns from the SOL of nebulin-deficient mice (Kiss et al., 2018). These muscles have a different fiber composition from wild type (∼90% type I, ∼10% type IIA), similar to rat SOL. While the results were variable, two of six muscles with good myosin layer lines showed substantially more lattice sampling than wild type (both 1,0 and 1,1 reflections; Fig. S7, C and D), but in no case were they as clear as in rat SOL. The relative weakness of simple lattice sampling in mouse SOL and absence of lattice sampling in EDL (Fig. S8) suggest that the lattices present in both muscles are not as ordered as in the rat.

We wanted to use electron microscopy of transverse sections of the bare region to confirm the lattice arrangement present in different fiber types of the mouse, as we did for rat (Figs. 3 and 4). We focused on the mouse SOL because of its mixture of fast and slow fibers. However, it is not possible to definitively identify fiber type in a mixed muscle based on transverse EM sections alone. One ultrastructural indicator of fiber type in transverse sections is the number of mitochondrial bundles lying immediately beneath the sarcolemma and in longitudinal arrays parallel to the myofibrils (Schiaffino et al., 1970; Gauthier, 1986; Schiaffino and Reggiani, 2011). These are common in slow type I and fast type IIA fibers, and absent from fast type IIB/D/X fibers. Using this feature as a guide, we attempted to distinguish type I/IIA from type IIB/D/X fibers in low-magnification electron micrographs of mouse SOL. We then examined filament orientation at high magnification in bare regions of fibers identified in this way. Statistical analysis of relative filament orientations, similar to that carried out in Figs. 4 and S5, showed that putative "fast" fibers of the SOL (those with minimal mitochondrial bundles: IIB/D/X) had a mean deviation angle of 33.1° when comparing filaments within a hexagon (Fig. S9 A). As discussed for rat, this is consistent with a no-three-alike superlattice, in which two of every three adjacent filaments have the same angle and the third is rotated by 60° (Fig. 4 D). We also measured the relative orientations of pairs of adjacent filaments (cf. Figs. 4 E and S5 E). The results showed broad, similar height peaks for relative orientations close to 0 or 60°, supporting a no-three-alike superlattice in these fibers (Fig. S9 B). If the fibers in EDL (essentially all fast) have the same lattice, why is superlattice sampling not seen in the x-ray diffraction pattern (Fig. S6)? Even in the best example of a superlattice (frog; Huxley and Brown, 1967), the sampling is relatively weak (Fig. S4, A and B), apparently due to the limited extent/disorder of the lattice (Luther and Squire, 1980, 2014). We suggest that the lattice in mouse may be more disordered than of rat or frog, and possibly also easily disrupted during specimen preparation.

We carried out a similar analysis on the SOL fibers showing abundant mitochondria (assumed to be type I or IIA), where we expect a simple lattice. These showed a broad peak with an average deviation of 25.5° for filaments in a hexagon, higher than the 19.8° found for rat SOL (Fig. S9 C) and the 0° expected for a perfect simple lattice. This was initially surprising, given that the x-ray data for mouse SOL that suggested a (somewhat disordered) simple lattice (Figs. S6 and S7). However, direct observation of relative orientations in these fibers showed many regions of similarly oriented triangles (Fig. S10), interspersed with others showing varying angles. This suggests that a simple lattice is indeed present, but that it is local and does not carry across an entire myofibril. We tested this idea by computing pairwise relative orientations as carried out for rat SOL and EDL and mouse SOL fast fibers. The results showed a substantially greater fraction of filaments with deviations close to 0° than close to 60°, clearly different from rat EDL and mouse SOL fast fibers, where the 0° and 60° had similar numbers. This supports the concept of local regions of simple lattice (Fig. S9 D) rather than a random orientation of filaments, which would predict an even distribution of rotations from 0 to 60°. A disordered (i.e. local) simple lattice would be expected to give an x-ray diffraction pattern with sampling on the 1,0 and 1,1 row lines, but the sampling would be weaker/more diffuse than for a perfect lattice, consistent with the observed weak sampling for the mouse SOL.

We conclude that, overall, analysis of mouse SOL (by x-ray diffraction and EM) and mouse EDL (by x-ray diffraction) supports the general conclusion that low-fatigue fibers (type I and IIA) have a simple lattice while fatigable fibers (type IIB, D, and X) have a superlattice. In no case is the lattice perfect: all have some degree of disorder (i.e., are limited in their extent).

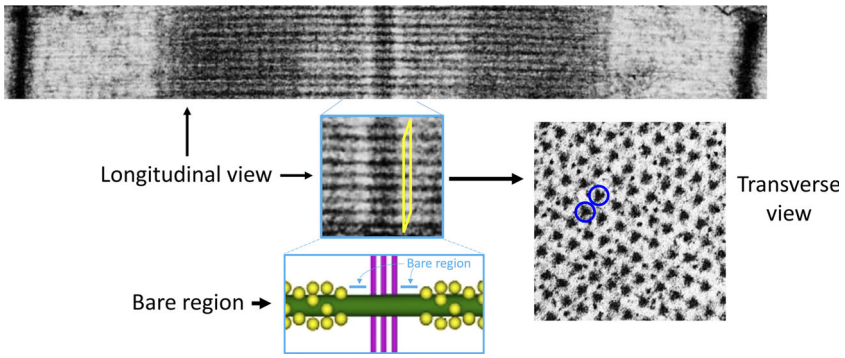


Figure S1. **Transverse sectioning of the "bare regions" of the thick filament.** Transverse sections of fixed and embedded muscle were cut and examined specifically in myofibrils where the thick filaments showed triangular profiles (examples in blue circles). This occurs in the bare regions (yellow parallelogram) of the thick filament bare zone, where M-line bridges (magenta) and myosin heads (yellow) are both absent (cartoon).

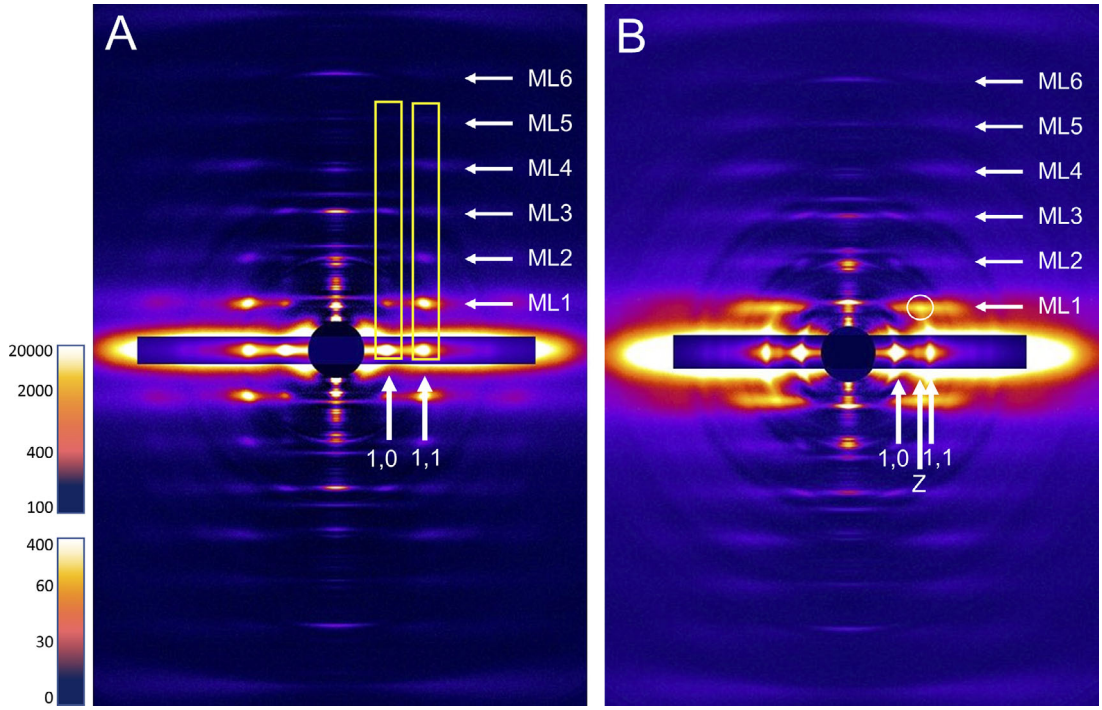


Figure S2. **X-ray diffraction patterns of skinned rat SOL and EDL.** Compare with live patterns in Fig. 2. **(A)** SOL: Note clear lattice sampling on ML1 and higher layer lines at positions aligning with 1,0 and 1,1 equatorial reflections (compare Fig. 2 A). **(B)** EDL: Note much weaker lattice sampling and alignment of strongest (diffuse) spot on ML1 with Z-line reflection on equator (compare Fig. 2 B), consistent with superlattice. Note strong similarity to live patterns in Figs. 2 and S3. Scale at left is intensity in arbitrary units (upper, equator; lower, rest of pattern).

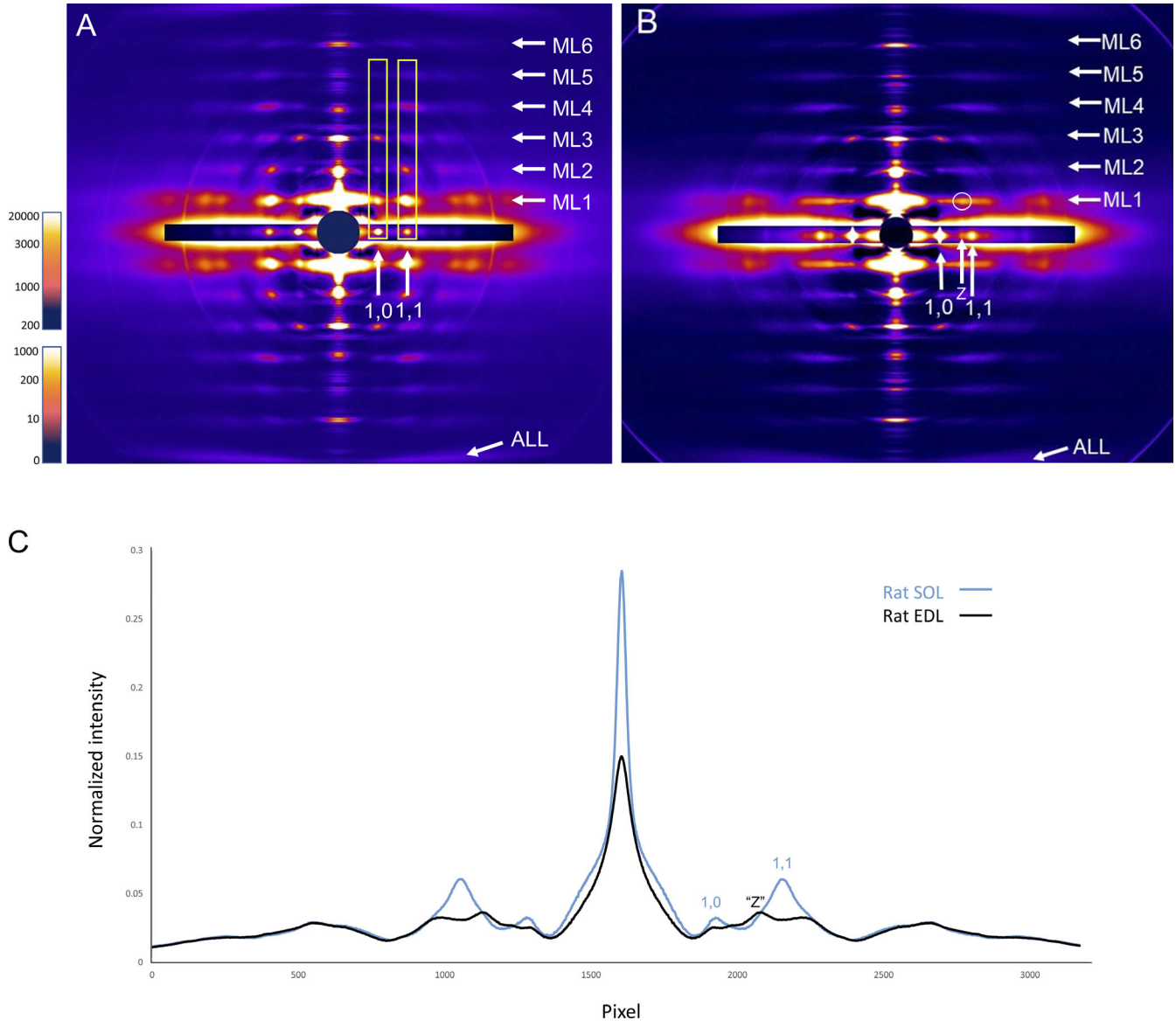


Figure S3. **X-ray diffraction patterns of rat SOL and EDL (from Fig. 2) with intensity plot of first myosin layer line. (A and B)** In SOL (A) and EDL (B), ML1–6 indicate positions of myosin layer lines (repeat 43 nm), and ALL indicates actin 5.9-nm layer line. Horizontal inserts on equator show shorter exposures to reveal the high-intensity equatorial 1,0 and 1,1 reflections. **(C)** Intensity plot of ML1 in SOL and EDL. Prominent lattice sampling is seen in SOL at 1,0 and 1,1 radial positions (A and C), indicating a simple lattice of myosin filaments. Lattice sampling is weak in EDL, and in a different position from SOL, on the inner side of the 1,1 reflection (B and C), aligning approximately with the Z-line reflection on the equator (see Figs. 2 and S4), consistent with a local superlattice with disorder. Scale at left in A and B is intensity in arbitrary units (upper, equator; lower, rest of pattern). In C, x axis is pixel number along the equator; central peak represents meridian.

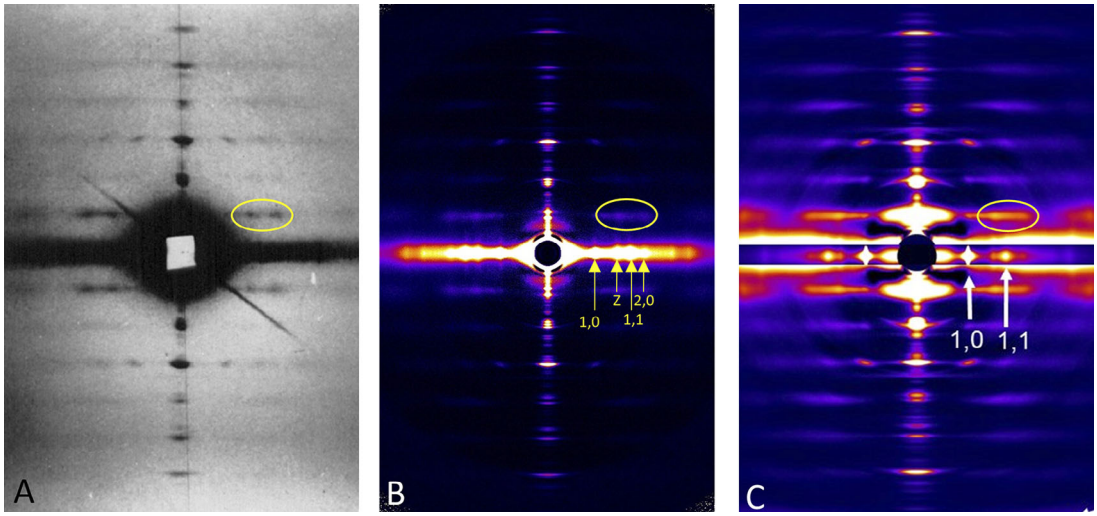


Figure S4. **X-ray diffraction patterns demonstrating superlattice arrangement of thick filaments. (A)** Frog sartorius muscle (from Huxley and Brown [1967], with permission). These authors first demonstrated the presence of a superlattice, based on the presence of the two reflections on the first layer line outlined by the yellow ellipse. **(B)** Frog sartorius muscle. Pattern taken on same beamline as the rat muscles in this paper showing superlattice sampling as in A (T. Irving and H.E. Huxley, unpublished data). **(C)** Rat EDL (this study, from Fig. 2 B) showing similar superlattice sampling in rat to that in frog.

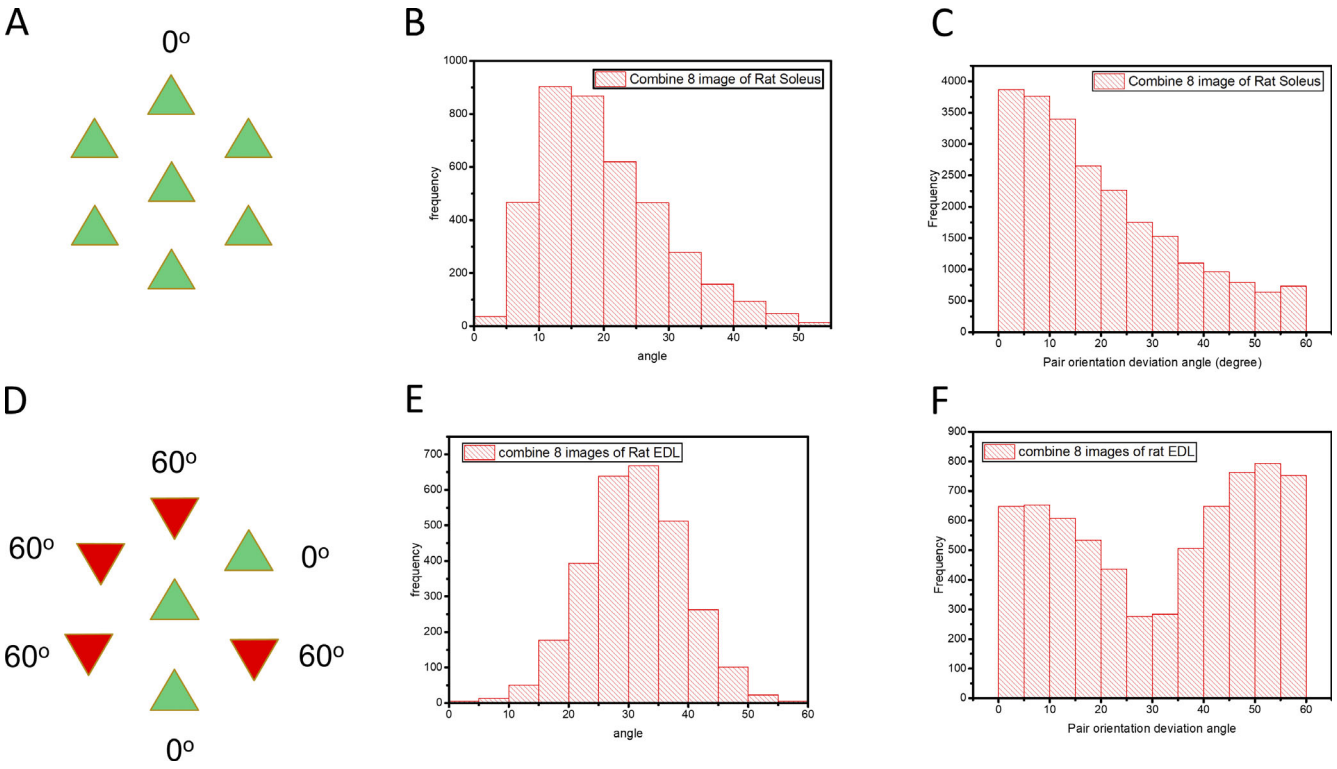


Figure S5. **Analysis of filament orientations in rat SOL and EDL, all data (see Fig. 4). (A and D)** Filament orientations in simple lattice (A; all filaments have same orientation; mean deviation angle = 0°) and in no-three-alike superlattice (D; in any group of three filaments, in a line or forming a triangle, one filament is rotated by 60° with respect to the other two, which are identical; mean deviation angle for any three adjacent filaments = 30°). **(B)** Histogram of mean deviation angle for the six filaments surrounding the central filament in a hexagon for all SOL micrographs analyzed. Average deviation angle = 19.8°, relatively close to the expected 0° for a simple lattice. The difference from 0° could have several sources. First, the curvature of the lattice in many of the micrographs exaggerates the deviation angle (see Fig. 4 legend). Second, there may be distortions of the lattice caused by muscle handling and EM processing, as well as natural variation within the muscle. Finally, there must inevitably be some deviation from the perfect 0° mean deviation angle for the six filaments surrounding a central filament, as the lattice is not perfect. Because we are using the absolute value of the deviation, the mean deviation for the six filaments must be a positive number, in this case 19.8°. **(C)** We determined whether this mean value is concealing individual measurements close to the expected 0° by calculating the deviation angle for neighboring filaments measured pairwise (Fig. 4 C). This gave a single peak with a maximum at 0°, as expected for a simple lattice, with the histogram tailing off out to 60°. Thus, the non-0° mean for the six filaments in a hexagon (B) arises from averaging filaments that have almost identical orientations (0°, as expected for a simple lattice) with those on the tail of the histogram, leading to the overall mean of 19.8°. **(E)** Mean deviation angle for the six filaments surrounding the central filament in a hexagon for all EDL micrographs analyzed. The average deviation angle is 30.9°, similar to the expected 30° for a superlattice. **(F)** Deviation angle for pairs of neighboring filaments in all EDL images analyzed. There are two peaks, close to 0 and 60°, as expected for a no-three-alike superlattice (see C). Note that the pairwise comparison for the SOL (C) is dramatically different from that for the EDL (F), further supporting the different lattices in SOL and EDL.

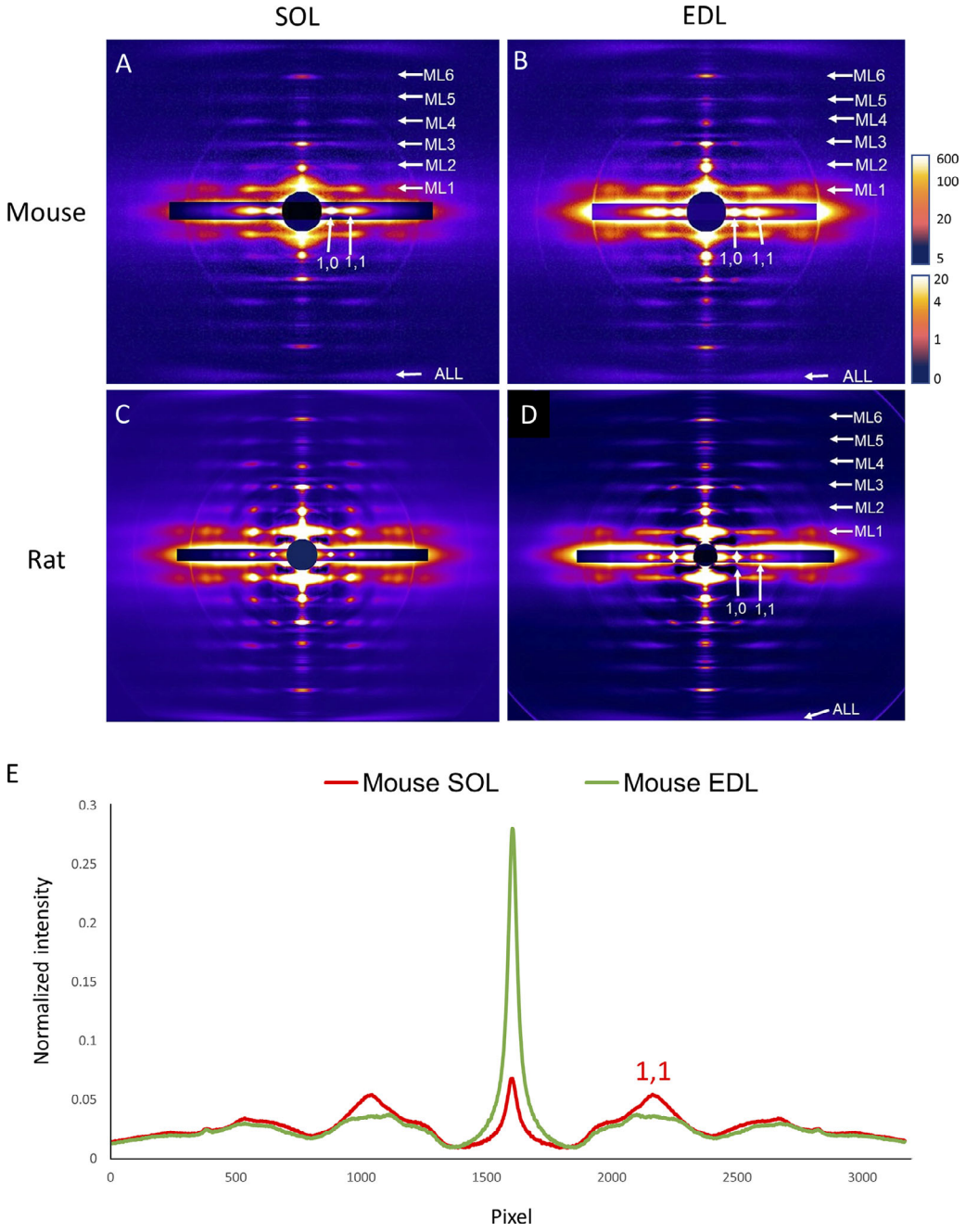


Figure S6. **X-ray diffraction patterns of mouse and rat SOL and EDL. (A–E)** X-ray diffraction patterns of mouse SOL (A) and EDL (B) compared with rat SOL (C) and EDL (D; from Fig. 2), with intensity plot of first myosin layer line in mouse (E). ML1–6 indicate positions of myosin layer lines (repeat 43 nm), and actin 5.9-nm layer line (ALL). 1,0 and 1,1 show positions of 1,0 and 1,1 equatorial reflections. Mouse EDL shows a relatively continuous density on ML1 (B and E), while mouse SOL shows a mixture of continuous density with significant, slightly diffuse sampling at the 1,1 radial position (A and E). Sampling is stronger in the rat than the mouse (see Fig. S7). Scale at right in A–D is intensity in arbitrary units (upper, equator; lower, rest of pattern). In E, the x axis is pixel number along the equator; central peak represents meridian.

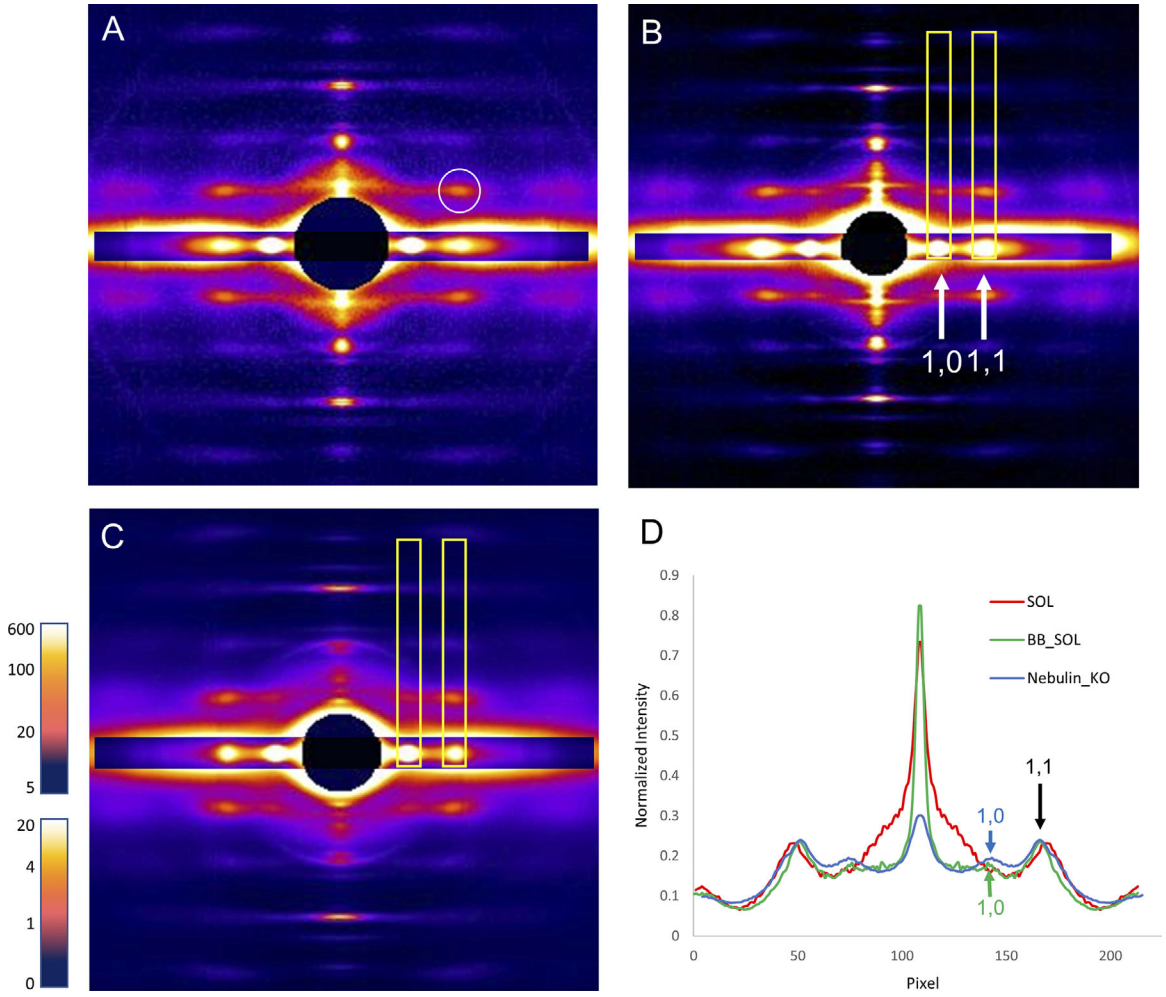


Figure S7. **X-ray diffraction of intact mouse SOL. (A and D)** Lattice sampling on ML1 (circle) is aligned with the 1,1 equatorial reflection, but there is no sign of 1,0 sampling (A; D, red trace). **(B and D)** Muscle treated for 30 min with blebbistatin (75 µM in Ringer solution) to see whether enhanced ordering of the heads (Xu et al., 2009) better reveals the lattice sampling. The lattice sampling became stronger and sharper, and a lattice spot on ML1 was now seen aligned with the 1,0 equatorial reflection (B, rectangles; D, green trace). **(C and D)** SOL from nebulin knockout mouse (Kiss et al., 2018), which is ∼90% type I and ∼10% type IIA (similar to rat SOL). The 1,1 sampling on ML1 is again clear and weak sampling now appears at the 1,0 position (C, rectangles; D, blue trace). Scale at left is intensity in arbitrary units (upper, equator; lower, rest of pattern). **(D)** Intensity plot of first myosin layer line in A–C. X axis is pixel number along the equator; central peak represents meridian. Red, wild-type SOL; green, SOL treated with blebbistatin; blue, SOL from nebulin knockout mouse.

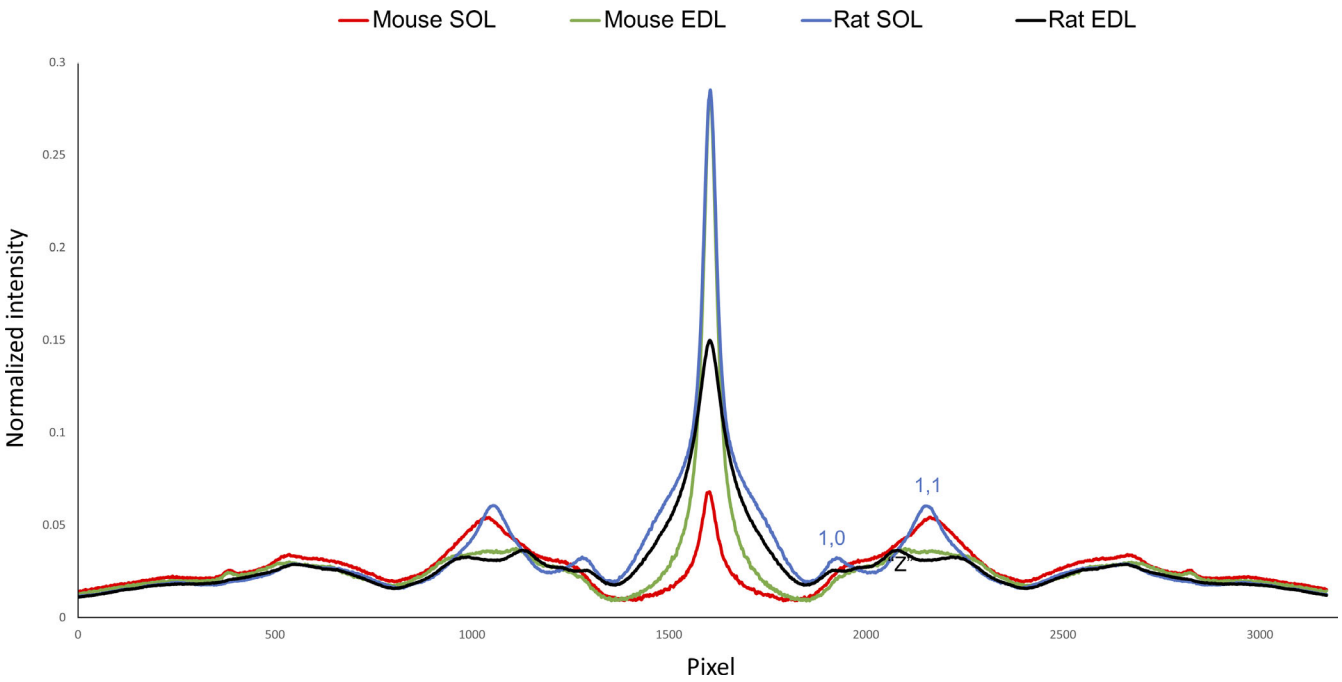


Figure S8. **Comparison of intensity plots of ML1 in rat and mouse SOL and EDL.** Both SOL muscles show a peak in line with the 1,1 equatorial reflection. The peak with rat is sharper than with mouse. Rat also shows a peak at the 1,0 radial position. Sampling with the EDL muscles is weaker. However, the rat shows a small but clear peak in line with the Z-line equatorial reflection, on the inner side of the 1,1, and another peak on the outer side of the 1,1. These reflections are characteristic of a superlattice (see Fig. S4). The y axis is normalized intensity (arbitrary units), and the x axis is pixel number along the equator; central peak represents meridian.

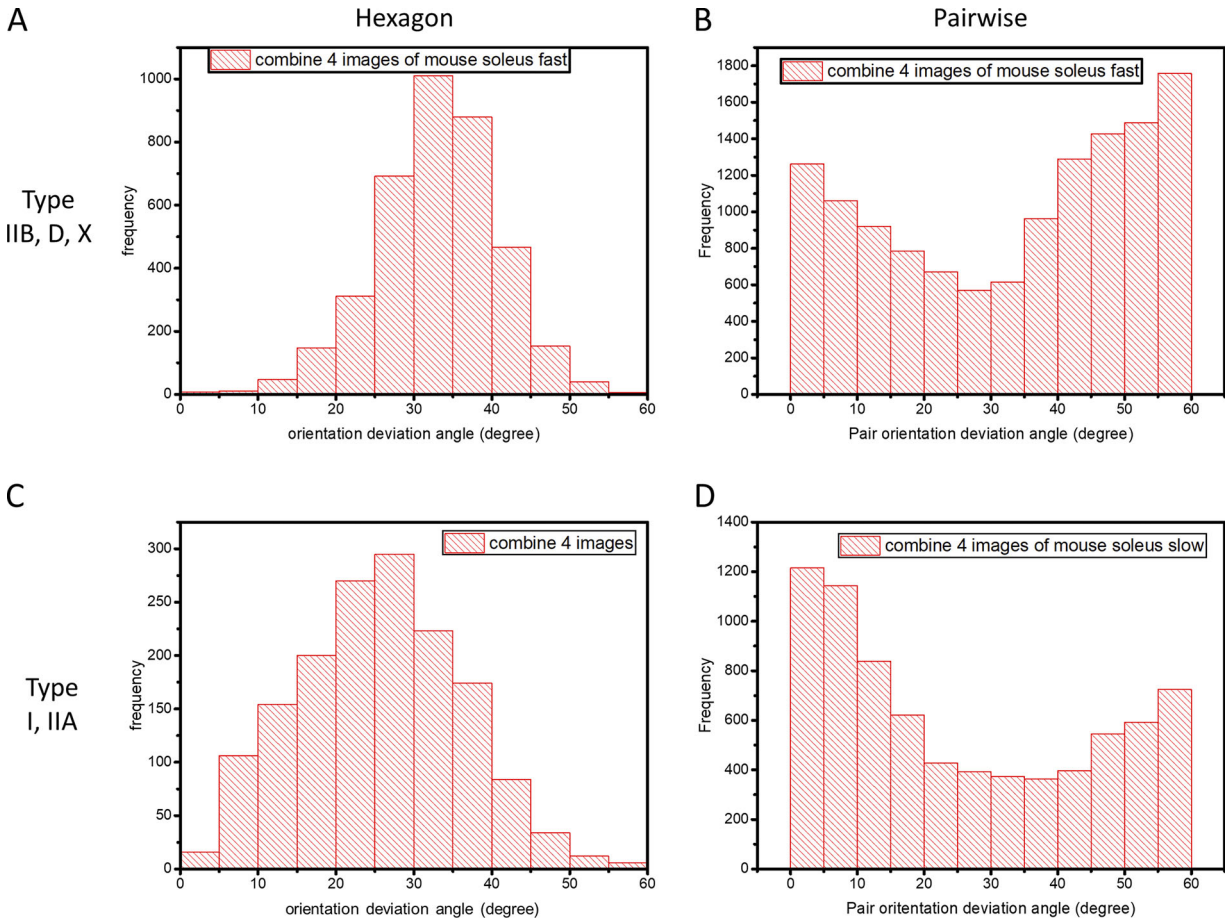


Figure S9. **Average angular deviation of mouse SOL thick filaments in fast (type IIB, D, and X) and slow (type I) and fast (type IIA) fibers. (A and C)** Average deviation for filaments in hexagons centered on the reference filament (compare Fig. S5, B and D). **(B and D)** Pairwise comparison of filaments. Note that A and C have average deviation angles of 30.9 and 25.5°, respectively. For the pairwise comparison, B has peaks of similar heights, close to 0 and 60°, as expected for a no-three-alike superlattice, while D shows a substantially higher peak close to 0° than that at 60°, more consistent with a limited extent/disordered simple lattice (see Fig. S10).

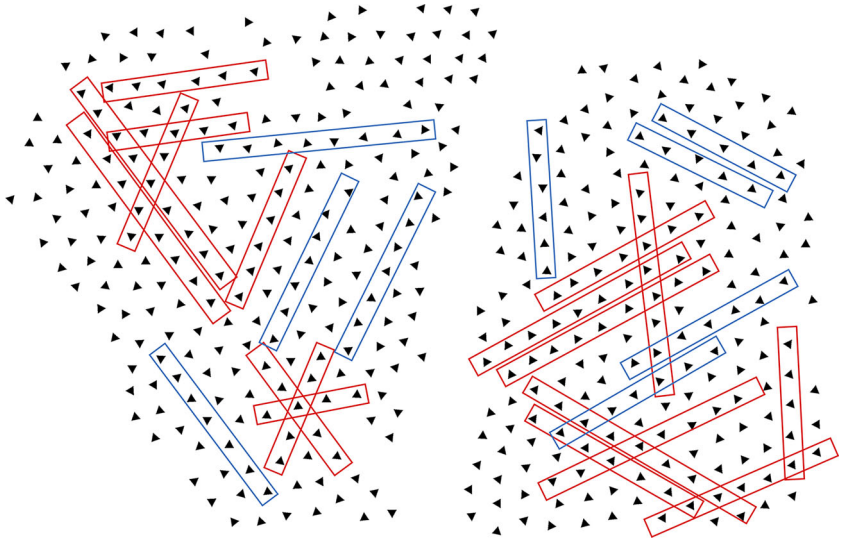

Figure S10. **Thick filament orientations in type I/IIA fibers of mouse SOL.** Fiber type was tentatively identified as type I/IIA based on high mitochondrial content. Thick filament orientations in two myofibrils were determined using the same methods as for Fig. 3 (D and F). Rectangles show local regions where filaments have similar orientations (simple lattice; red) interspersed with varying orientations (blue).

## References


Augusto, V., C.R. Padovani, and G.E.R. Campos. 2004. Skeletal muscle fiber types in C57BL6J mice. *Braz. J. Morphol. Sci.* 21:89–94.

Gauthier, G.F. 1986. Skeletal muscle fiber types. *In* Engel, A.G., and B.Q. Banker, editors. *Myology*. McGraw-Hill Book Company, New York; 255–283.

Huxley, H.E., and W. Brown. 1967. The low-angle x-ray diagram of vertebrate striated muscle and its behaviour during contraction and rigor. *J. Mol. Biol.* 30: 383–434. https://doi.org/10.1016/S0022-2836(67)80046-9

Iwamoto, H., J. Wakayama, T. Fujisawa, and N. Yagi. 2003. Static and dynamic x-ray diffraction recordings from living mammalian and amphibian skeletal muscles. *Biophys. J.* 85:2492–2506. https://doi.org/10.1016/S0006-3495(03)74672-4

Kiss, B., E.J. Lee, W. Ma, F.W. Li, P. Tonino, S.M. Mijailovich, T.C. Irving, and H.L. Granzier. 2018. Nebulin stiffens the thin filament and augments cross-bridge interaction in skeletal muscle. *Proc. Natl. Acad. Sci. USA.* 115:10369–10374. https://doi.org/10.1073/pnas.1804726115

Li, A., S.R. Nelson, S. Rahmanseresht, F. Braet, A.S. Cornachione, S.B. Previs, T.S. O'Leary, J.W. McNamara, D.E. Rassier, S. Sadayappan, et al. 2019. Skeletal MyBP-C isoforms tune the molecular contractility of divergent skeletal muscle systems. *Proc. Natl. Acad. Sci. USA.* 116:21882-21892. https://doi:10.1073/pnas.1910549116.

Luedeke, J.D., R.D. McCall, R.M. Dillaman, and S.T. Kinsey. 2004. Properties of slow- and fast-twitch skeletal muscle from mice with an inherited capacity for hypoxic exercise. *Comp. Biochem. Physiol. A Mol. Integr. Physiol.* 138:373–382. https://doi.org/10.1016/j.cbpb.2004.05.010

Luther, P.K., and J.M. Squire. 1980. Three-dimensional structure of the vertebrate muscle A-band. II. The myosin filament superlattice. *J. Mol. Biol.* 141:409–439. https://doi.org/10.1016/0022-2836(80)90254-5

Luther, P.K., and J.M. Squire. 2014. The intriguing dual lattices of the myosin filaments in vertebrate striated muscles: evolution and advantage. *Biology (Basel).* 3:846–865. https://doi.org/10.3390/biology3040846

Schiaffino, S., and C. Reggiani. 2011. Fiber types in mammalian skeletal muscles. *Physiol. Rev.* 91:1447–1531. https://doi.org/10.1152/physrev.00031.2010

Schiaffino, S., V. Hanzlíková, and S. Pierobon. 1970. Relations between structure and function in rat skeletal muscle fibers. *J. Cell Biol.* 47:107–119. https://doi.org/10.1083/jcb.47.1.107

Totsuka, Y., Y. Nagao, T. Horii, H. Yonekawa, H. Imai, H. Hatta, Y. Izaike, T. Tokunaga, and Y. Atomi. 2003. Physical performance and soleus muscle fiber composition in wild-derived and laboratory inbred mouse strains. *J. Appl. Physiol.* 95:720–727. https://doi.org/10.1152/japplphysiol.00946.2002

Wigston, D.J., and A.W. English. 1992. Fiber-type proportions in mammalian soleus muscle during postnatal development. *J. Neurobiol.* 23:61–70. https://doi.org/10.1002/neu.480230107

Xu, S., H.D. White, G.W. Offer, and L.C. Yu. 2009. Stabilization of helical order in the thick filaments by blebbistatin: further evidence of coexisting multiple conformations of myosin. *Biophys. J.* 96:3673–3681. https://doi.org/10.1016/j.bpj.2009.01.049